Phase diagrams and magnetic excitations in holmium phosphide

P. Fischer and A. Furrer
Labor für Neutronenstreuung, Eidgenössische Technische Hochschule Zürich, CH-5303 Würenlingen, Switzerland

E. Kaldis
Laboratorium für Festkörperphysik, Eidgenössische Technische Hochschule Zürich, CH-8093 Zürich, Switzerland

D. Kim
Department of Physics, Seoul National University, Seoul 151, Korea

J. K. Kjems
Physics Department, Risø National Laboratory, DK-4000 Roskilde, Denmark

P. M. Levy
Department of Physics, New York University, 4 Washington Place, New York, New York 10003
(Received 25 June 1984)

New neutron scattering studies were made on holmium phosphide (HoP) in order to resolve existing ambiguities. Neutron-diffraction investigations were performed on single-crystal and powdered samples of HoP in external fields up to 40 kOe as well as in zero field. In addition to obtaining phase diagrams, we have determined that the easy directions of magnetization are ⟨100⟩ in the ferromagnetic and paramagnetic states. Depending on the history of the samples, structural defects presumably of Schottky type tend to shorten the range of magnetic order. Inelastic neutron scattering was used to measure the magnetic excitation spectrum of HoP in the flopside phase. Four spin-wave branches were found which are almost independent of wave vector. The results are analyzed in terms of a mean-field Hamiltonian containing a crystal field and the effects of bilinear and quadrupolar pair interactions. On the basis of the resulting model parameters, we are able to explain the salient features of the magnetic behavior of HoP, in particular, the appearance of first the ferromagnetic and then the flopside phases, and the variations with fields of the paramagnetic-flopside transitions and the flopside-ferromagnetic transitions.

I. INTRODUCTION

Holmium phosphide (HoP) belongs to the rare-earth monopnictides which have a rocksalt structure. At $T_C=5.4$ K it undergoes a second-order phase transition and orders ferromagnetically.[1] There is a first-order phase transition at $T_F=4.8$ K from the ferromagnetic to a flopside phase[1,2] in which the fcc lattice of holmium ions breaks up into two sublattices each one consisting of alternate (111) planes. The sublattice magnetizations $\vec{M}_A$ and $\vec{M}_B$ are approximately oriented along cube edges and perpendicular to one another. In the subsequent analysis we assume equivalent sublattices, i.e., $\vec{M}_A=(M_x,M_y,0)$ and $\vec{M}_B=(M_y,M_x,0)$. HoP has strong crystal fields; the parameters as determined by neutron spectroscopy[3,4] ($W=-0.025$ meV and $x=0.75$) are such that the six lowest-lying states of the ground-state multiplet $^5I_8$ of Ho^{3+} are nearly degenerate and well separated from the other levels. This level scheme forms the basis of the cubic model.[5]

The magnetic behavior of HoP was recently studied within the cubic-model approximation,[5] and the appearance of first a ferromagnetic and then a flopside phase was ascribed to two features of the model. First, a weak intersublattice coupling due to competing first- and second-neighbor bilinear interactions, and second, appreciable antiferroquadrupolar pair interactions. At the time it was not possible to determine a *unique* set of model parameters; only conditions that the parameters must satisfy were found. To determine these parameters we measured the magnetic excitation spectra of HoP by means of inelastic neutron scattering. An analysis of these data based on the Hamiltonian used to understand the magnetothermal behavior of HoP has yielded a unique set of parameters.

Also, as previous neutron diffraction studies were made in zero field, the easy directions in the ferromagnetic state were not known. According to the theory[5] either ⟨100⟩ or ⟨111⟩ was possible. To resolve this, neutron-diffraction measurements were made in HoP in external fields (a brief summary of the results is published in Ref. 1). In addition to answering this question, recently performed single-crystal studies have provided us with phase diagrams of HoP in external fields.

In Sec. II we describe these neutron-diffraction studies and the results. The inelastic neutron-scattering experiments used to determine the magnetic excitation spectra of HoP and the analysis used to determine the model parameters are described in Sec. III. By using the model Hamiltonian previously developed for HoP, and the parameters determined in Sec. III, we describe in Sec. IV a

mean-field analysis of the phase behavior of HoP in external fields. We summarize our findings in the last section.

II. NEUTRON DIFFRACTION: MAGNETIC PHASES

A. Samples

The sample preparation has been previously described.[6] The characteristic properties of the specimens used in the neutron-diffraction investigations are summarized in Table I. The holmium content was determined by chemical analysis. Apparently the lattice constant depends to a large measure on sample perfection. Most neutron-diffraction investigations were made on stoichiometric samples ($S2$,$P2$). The single-crystal $S2$ has approximate dimensions $(1.5-3.5)\times 2.5\times 2.5$ mm^3 (the latter edge is parallel to [001]). The samples were enclosed in cylindrical vanadium or aluminum containers (1 cm in diameter for powders) under a pure helium atmosphere.

B. Experiments

Elastic neutron-scattering experiments were performed on two-axis spectrometers at the reactor Saphir in Würenlingen. Without external magnetic fields neutron wavelengths of $\lambda=0.9$ Å (Er filter) and 2.34 Å were used in cases of single crystals and powders, respectively. The powder sample $P2$ was also measured at $\lambda=1.06$ Å in external magnetic fields $\vec{H}$ with magnitudes up to 8.3 kOe, using an electromagnetic and a variable temperature cryostat. The magnetic field was oriented parallel to the scattering vector $\vec{Q}$. This method permits the determination of the easy direction of magnetization also for cubic systems.[2] Although there might arise some problems in such measurements due to preferred orientations, the main advantage of using powders in the present case is the absence of extinction. This would be particularly associated with magnetic intensities because of the large magnetic moment of Ho^{3+} ($\sim 10\mu_B$). For the determination of magnetic phase diagrams the single-crystal $S2$ was mounted in a superconducting magnet with magnetic field perpendicular to the scattering plane. By means of a two-axis spectrometer equipped with a tilting counter fields parallel [001] and [0$\bar{1}$1] could be studied. For this purpose the crystal was glued on an aluminum sample holder permitting changes of orientation. The temperature was controlled by means of a field-independent capacitance sensor. Powder diffraction patterns corrected for absorption were analyzed by means of the profile method,[7] using scattering lengths $b_{Ho}=0.808\times 10^{-12}$ cm $b_P=0.513\times 10^{-12}$ cm,[8] and a relativistic neutron magnetic form factor f for Ho^{3+} in the dipole approximation.[9]

C. Results

1. *Long-range magnetic order in zero magnetic field*

In Fig. 1 we show typical neutron-diffraction patterns of HoP as function of temperature. In the paramagnetic state at 7.0 K one observes only nuclear Bragg peaks. The large intensity increase of weak nuclear reflections such as 1 1 1 and the absence of any additional peaks clearly indicate the existence of long-range ferromagnetic order in HoP at 5.0 K. As no deviations from cubic symmetry are observed, only the magnitude of the ordered magnetic moment $\vec{\mu}$ of Ho may be derived from this diagram. At 4.2 K the diffraction pattern contains both large ferromagnetic and antiferromagnetic Bragg intensities which confirm the flopside model.[2] Assuming two equivalent magnetic sublattices $\vec{\mu}_A$ and $\vec{\mu}_B$, the ferromagnetic intensities depend on the magnitude of the vector $\vec{\mu}_+=\vec{\mu}_A+\vec{\mu}_B$ which is oriented parallel to the direction [110]. The antiferromagnetic peaks yield information both on the magnitude of $\vec{\mu}_-=\vec{\mu}_A-\vec{\mu}_B$ (in the model parallel to [1$\bar{1}$0], i.e., perpendicular to [111]) and on the angle of $\vec{\mu}_-$ with respect to the cubic [111] direction.[1] Thus it is possible to determine both components μ_x and μ_y. At 4.2 K the fit of observed and calculated profile intensities is shown in Fig. 2. The refined structural parameters are summarized in Table II. Scale factors were determined in the paramagnetic state from the nuclear intensities. The overall temperature factor B decreased from 0.09(8) Å^2 at

TABLE I. Characteristic properties of the HoP samples used in the neutron-diffraction studies. S denotes a single crystal, P a powder.

Sample	Annealing temperature (°C)	X-ray lattice constant (Å)	Ho content (percent of theoretical value by weight)	Magnetic ordering
$S1$	2500	5.604	100.8	Short-range order
$S2$	1400	5.624	100.3	Flopside structure, ferromagnetism
$P1$[a]	1400	5.624	96	Flopside structure
$P2$	1600	5.627	100.6	Flopside structure, ferromagnetism
$P3$	2100	5.614	86.9	Short-range order (predominant)

[a]Measured at temperature $T\leq 4.2$ K.

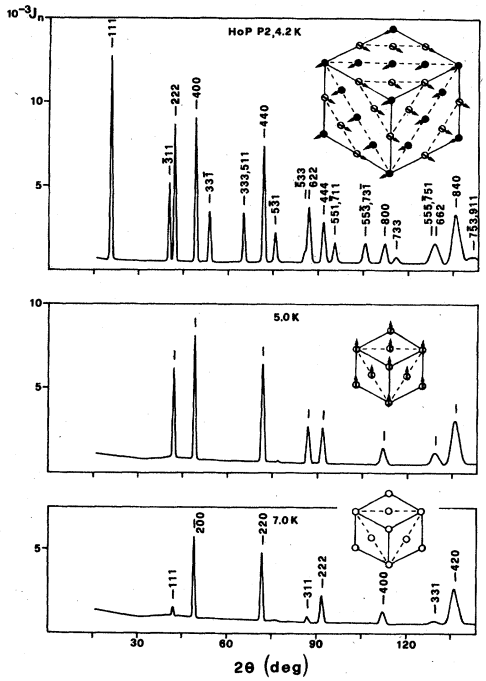

FIG. 1. Temperature dependence of neutron-diffraction pattern of the HoP powder sample $P2$. At 4.2 K the indexing corresponds to the magnetic unit cell with lattice constant $a_m = 2a$. Inserts indicate corresponding magnetic structures.

293 K to $-0.13(4)$ Å^2 at 4.2 K. Presumably the latter negative value corresponds to residual errors in absorption corrections and estimates of the background. The values of the parameters change only within standard deviations, if B is set equal to zero. The temperature dependence of μ_x and μ_y, see Fig. 3, was determined from the measured integrated intensities of the reflections 1 1 1, $\frac{1}{2}\frac{1}{2}\frac{1}{2}$, and $\frac{3}{2}\frac{1}{2}\frac{1}{2}$ (with respect to the chemical cell). The moments are normalized to the more accurate values obtained by profile refinement, see Table II. Concerning transition temperatures more precise new single-crystal results are shown in Fig. 4. We use inflection points for the definition of transition temperatures. In particular this holds for T_C, where critical scattering is expected.

Maxima of diffuse magnetic intensity were indeed observed at temperatures near T_C in the vicinity of reflections 1 1 1 and $\frac{1}{2}\frac{1}{2}\frac{1}{2}$. From Fig. 4 we find a Curie temperature $T_C = 5.4(1)$ K, in good agreement with that reported in previous studies.[1,2] The phase transition appears to be of second order. At $T_F = 4.8(1)$ K there is a first-order phase transition from ferromagnetism to a flopside configuration. At T_F a small hysteresis of the order of 0.07 K is observed.

2. *Magnetic short-range order caused by defects*

In the single-crystal sample $S1$ only short-range antiferromagnetic intensity was observed in the vicinity of the $\frac{1}{2}\frac{1}{2}\frac{1}{2}$ peak position for the temperature range from 1.4 to 4.2 K. At the same time the integrated intensity of the nuclear reflection 1 1 1 remained constant.[1] As the single-crystal $S1$ was synthesized and annealed at high temperatures of the order of 2500°C, see Table I, the creation of a substantial number of Schottky defects is probable, which presumably tends to shorten the range of magnetic order in zero field.

Further evidence for the important influence of defects

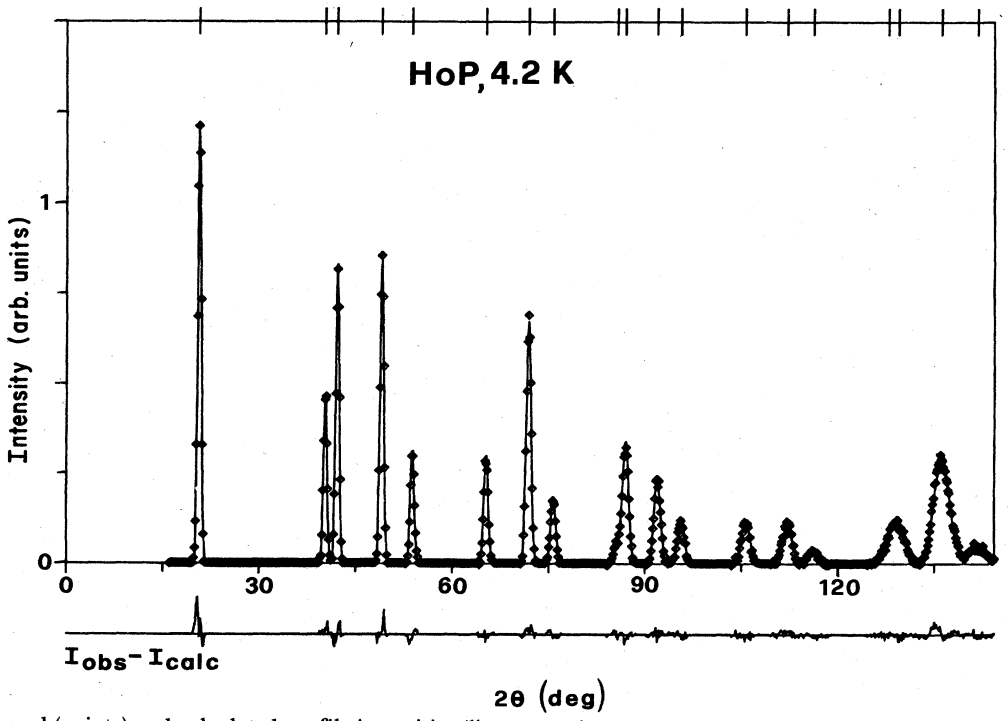

FIG. 2. Observed (points) and calculated profile intensities (line, assuming a cubic lattice) of polycrystalline HoP $P2$ at 4.2 K in the flopside phase.

TABLE II. Refined lattice constant a, ordered magnetic moment $\vec{\mu}=(\mu_x,\mu_y,0)$ of Ho^{3+}, and agreement values R, RW_p, see Ref. 7, for the HoP powder sample $P2$. Temperature is denoted by T. Standard deviations are given in the parentheses. The magnetic moment for the slightly nonstoichiometric sample $P1$ ($HoP_{0.94(1)}$ according to neutron intensities) at 4.2 K is $\mu_x=7.40(4)\mu_B$ and $\mu_y=0.33(4)\mu_B$.

T (K)	a (Å)	μ_x (μ_B)	μ_y	μ	R_n	R_m	RW_p
293	5.627(7)				0.033		0.111
7.0	5.620(7)				0.024		0.083
5.0	5.622(7)			5.18(3)	0.017	0.019	0.062
4.2	5.617(7)	9.16(4)	0.18(3)	9.16(4)	0.025	0.035	0.098

on the magnetic properties of HoP was obtained on a similar powder sample which also deviates from 1:1 stoichiometry, see Table I, $P3$ ($HoP_{0.94(1)}$ according to neutron intensities). Sections of corresponding neutron-diffraction patterns are shown in Fig. 5. Compared to Fig. 1 the coherent magnetic intensity due to long-range order appears to be very weak even at 4.2 K; the ordered magnetic moment of holmium μ_{Ho} is about $0.9\mu_B$. The magnetic scattering is mainly incoherent, corresponding to broad diffuse peaks, e.g., in the vicinity of $\bar{3}\,1\,1_m$, see Fig. 5. Such "critical" modulations of the paramagnetic intensity which is proportional to $f^2(Q)$, indicate short-range magnetic correlations, similar to those found in TbSe.[10] The differences in the saturation values of ordered magnetic moments of different HoP samples, see Fig. 3, appear to depend mainly on Schottky defects (possible on both anion and cation sites), corresponding to the annealing temperature. Nonstoichiometry seems to be of secondary importance. In contrast to chemical analysis, see Table I, neutron intensities indicate both for sample $P1$ and $P3$ the composition $HoP_{0.94}$. Presumably the concentrations of Schottky defects in these specimens are different. Another difference is the presence of an impurity phase in sample $P3$, see Fig. 5. On the other hand, in the case of the stoichiometric powder sample $P2$ the free-ion value of $10\mu_B$ for the ordered magnetic moment per Ho^{3+} ion is nearly attained at low temperatures $\mu_0=9.7(1)\mu_B$, i.e., corresponding crystal-field effects are weak. This is in perfect agreement with calculation, cf. Fig. 14.

3. *Effects of external magnetic fields*

In order to determine magnetic phase diagrams the HoP single-crystal $S2$ was investigated in external magnetic fields H up to 4 T (40 kOe) and within the temperature range from approximately 2 to 10 K. The orientation of the magnetic field along axes [001] and [0$\bar{1}$1] were studied. Generally we measured peak intensities as a function of decreasing temperature at various magnetic fields, i.e., starting from the paramagnetic state. We use inflection points for the definition of phase boundaries. Additional measurements were performed at constant temperature (reached from the paramagnetic state) as function of increasing and decreasing magnetic field. The resulting average phase diagrams are shown in Figs. 6 and 7. In the case of the [001] diagram all four ⟨111⟩ domains have the same angle of 54.7° with respect to the magnetic field, i.e., the normals to the ferromagnetic planes make this angle with respect to the field. For each ⟨111⟩ domain up to 12 different ⟨110⟩ orientations of $\vec{\mu}_\pm$ exist. In the case of the [0$\bar{1}$1] phase diagram the behavior of the [111] domain (perpendicular to $\vec{H}$) resem-

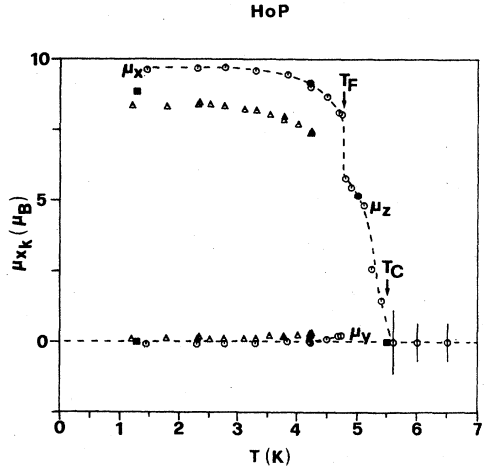

FIG. 3. Temperature dependence of ordered magnetic moment components μ_{x_k} of Ho^{3+} in polycrystalline HoP. Circles and triangles denote samples $P2$ and $P1$, respectively; squares represent data from Ref. 2. Solid symbols indicate results from profile fits.

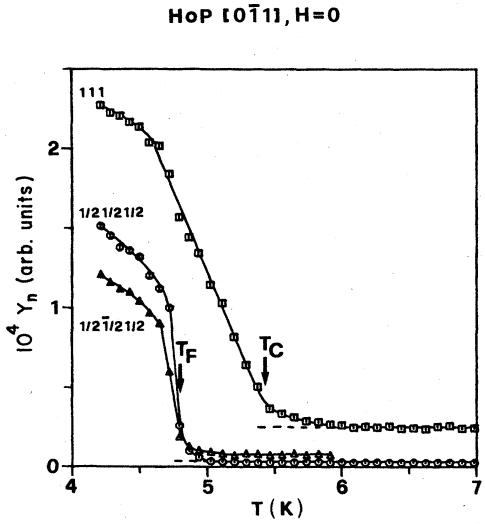

FIG. 4. Temperature dependence of neutron peak intensities of HoP single-crystal $S2$ on decreasing temperature (arbitrary units, external magnetic field $H=0$).

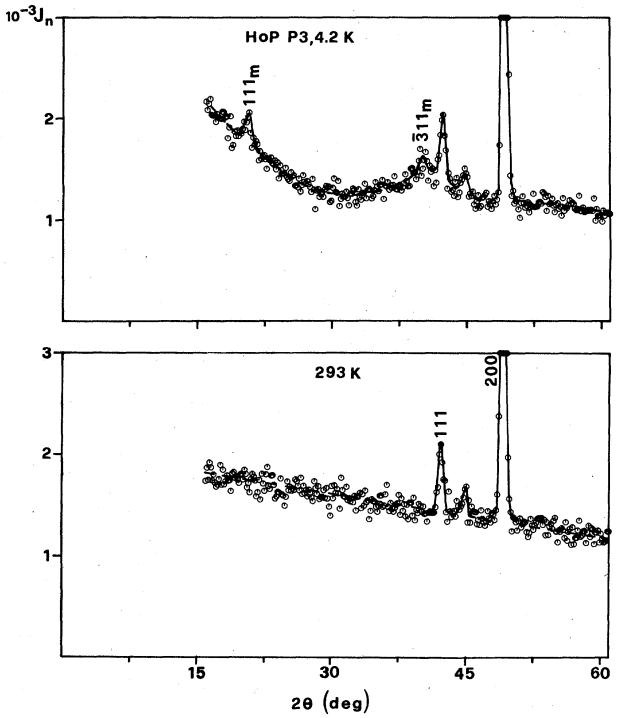

FIG. 5. Sections of the neutron-diffraction patterns of the HoP powder sample $P3$ illustrating predominant short-range correlations at 4.2 K, in comparison to the paramagnetic state at 293 K. The small peak at $2\theta \sim 45°$ originates from an unidentified impurity phase.

bles the [001] phase boundaries. On the other hand, the stable $[1\bar{1}1]$ domain, with angle 35.3° to $\vec{H}$, corresponding to sublattice magnetizations $\vec{\mu}_A \| \sim[0\bar{1}0]$ and $\vec{\mu}_B \| \sim[001]$, shows a marked field dependence; see Figs. 4, 7, and 8. In particular, the magnetic peak $\frac{1}{2}\frac{1}{2}\frac{1}{2}$ suggests a change from first-order transition in zero field to second-order transition in larger external magnetic fields ($\gtrsim 5$ kOe). Similar observations were made with magnetic fields oriented along [001]. In this context domain

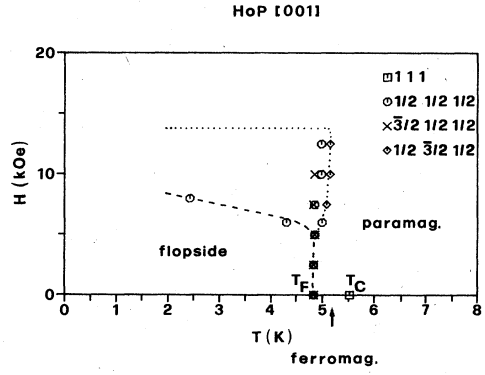

FIG. 6. Magnetic phase diagram of HoP for external magnetic field along a ⟨100⟩ direction. The points marked by symbols correspond to inflection points. The dashed and dotted lines indicate the boundaries within which the flopside phase disappears.

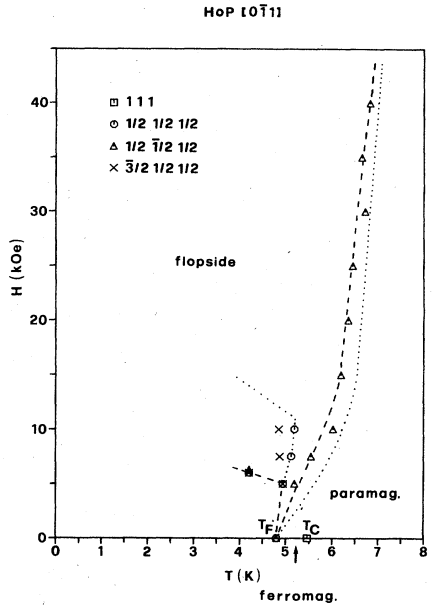

FIG. 7. Magnetic phase diagram of HoP for external magnetic field along a ⟨110⟩ direction. This diagram contains reflections from two inequivalent ⟨111⟩ domains; see text. The dashed and dotted lines indicate the boundaries within which the flopside phase (domains $[1\bar{1}1]$, [111]) goes over to the paramagnetic phase.

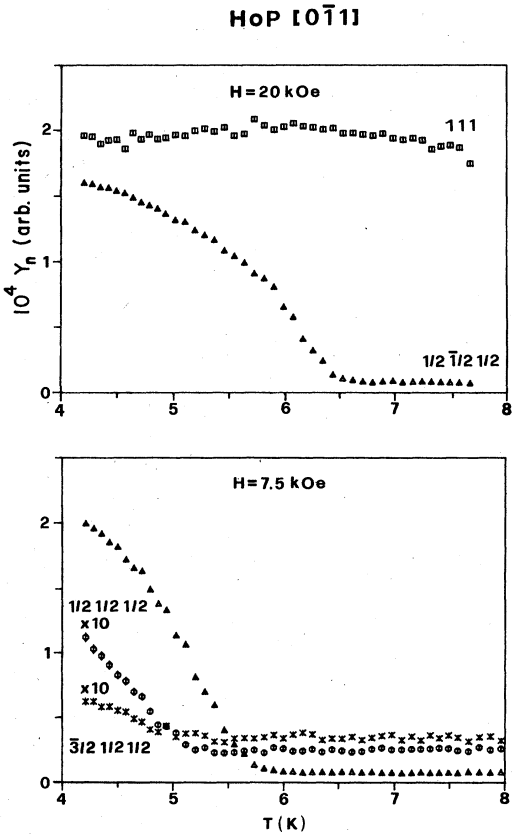

FIG. 8. Dependence of selected magnetic peak intensities of HoP single-crystal $S2$ on decreasing temperature, for external magnetic field $\vec{H} \| [0\bar{1}1]$.

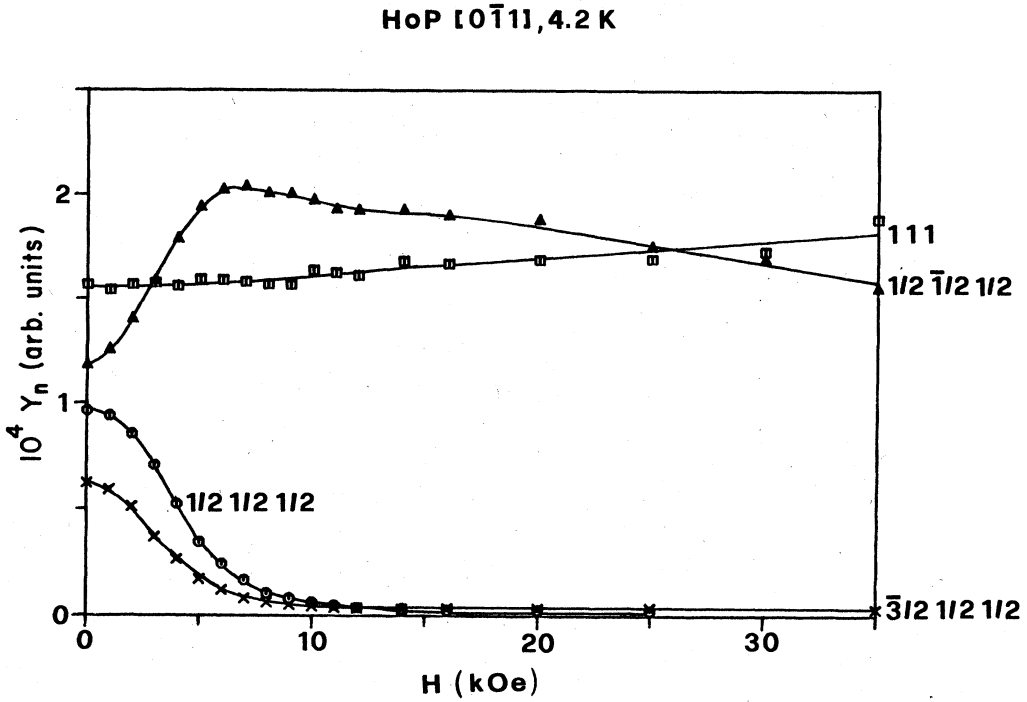

FIG. 9. Dependence of peak intensities of selected magnetic peaks of HoP single-crystal $S2$ on increasing magnetic field $\vec{H}||[0\bar{1}1]$ at 4.2 K.

reorientation effects are presumably important. An example of the magnetic field dependence of magnetic intensities is shown in Fig. 9. The transition to the ferromagnetic state appears to occur rather gradually. The 1 1 1 peak shown in Fig. 8, in particular the weak temperature dependence at $H=20$ kOe, characterizes a paramagnet in an external magnetic field and suggests a substantial induced moment. This is seen more clearly in Fig. 10, which shows the field dependence of the induced magnetic moment per Ho^{3+} ion in the paramagnetic state, calculated from the magnetic intensity of the 1 1 1 reflection (demagnetization corrections were neglected). In particular, these results indicate easy directions of magnetization $\langle 100\rangle$ in the paramagnetic state ($\mu[0\bar{1}1] \sim \mu[001]/\sqrt{2}$) in agreement with crystal-field considerations.

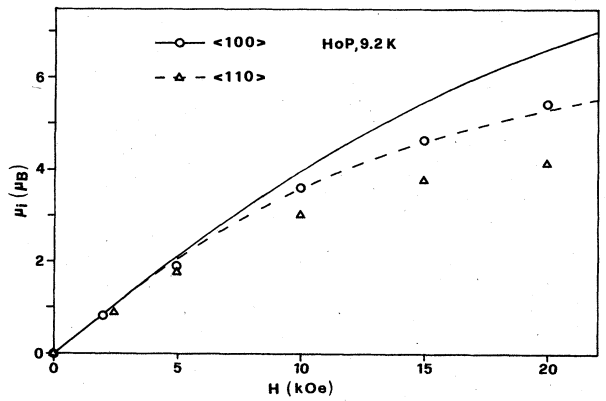

FIG. 10. Dependence of induced ferromagnetic moment on field in the paramagnetic HoP single-crystal $S2$ at 9.2 K: (a) for fields along [001]; (b) for fields along [0$\bar{1}$1]. We also show by lines the moments calculated from the 17-level scheme, see text, including corrections for demagnetization in the approximation of spherical shape. The differences between the observed and calculated values of the moments may be due to the irregular sample geometry.

In order to determine the easy directions of magnetization also in the ferromagnetic state, the powder sample $P2$, see Table I, was studied by means of neutron diffraction in external magnetic fields $\vec{H}$ ($H \leq 8.3$ kOe) oriented along the scattering vector $\vec{Q}$. Typical powder results are reproduced in Fig. 11. The measurement of the temperature dependence of reflection $\frac{3}{2}\frac{3}{2}\frac{1}{2}$ yields a shift of the phase boundary (T_F) between flopside phase and

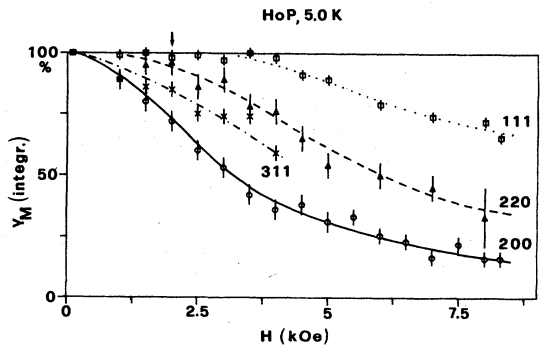

FIG. 11. Magnetic field dependence (increasing external field $\vec{H}$ parallel to $\vec{Q}$) of normalized integrated magnetic neutron intensities of the polycrystalline sample $P2$ of HoP at 5.0 K. The arrow indicates a phase boundary (ferromagnetism to flopside phase) for the [110] direction.

paramagnetic state from 4.8(1) K at $H=0$ to 5.0(1) K at 8.3 kOe for the magnetic field $\vec{H}$ parallel to [33$\bar{1}$]. The large decrease of magnetic neutron intensity for the 2 0 0 reflection, see Fig. 11, proves that the easy directions are ⟨100⟩ in ferromagnetic HoP. With respect to the limited magnetic field range of the ferromagnetic state of HoP at 5.0 K, we performed similar measurements at 5.3 K. In the latter case zero magnetic intensity was first attained in the Bragg peak 2 0 0 at approximately 6 kOe, which confirms that the easy directions of magnetization are ⟨100⟩. Effects due to induced magnetic moment were observed particularly for the reflection 1 1 1 in the sense that the intensity increases up to about 4 kOe.

D. Discussion

The present neutron-diffraction investigations on HoP prove the existence of a first-order magnetic phase transition from the flopside structure to the ferromagnetic phase at $T_F=4.8(1)$ K in zero magnetic field. Near T_F the component μ_y of the ordered magnetic moment per Ho^{3+} ion reaches its maximum value, but remains considerably smaller than μ_x. At saturation, a stoichiometric sample of HoP nearly attains its free-ion value of $10\mu_B$. The ferromagnetic-paramagnetic transition at $T_C=5.4(1)$ K is second order. At low temperatures ($\lesssim 1.7$ K),[2,11] in the ferromagnetic and paramagnetic states the easy directions of magnetization are ⟨100⟩. The transitions from the flopside phase to the ferromagnetic or paramagnetic states depends essentially on both directions and magnitude of the magnetic field. With increasing field this transition appears to change from first to second order, provided that effects due to magnetic domains do not simulate such a change. Depending on the thermal history of the samples and on the nonstoichiometry, structural defects presumably of the Schottky type have a profound influence on the lattice constants and magnetic properties of HoP, e.g., they break up long-range magnetic order.

III. INELASTIC NEUTRON SCATTERING: MAGNETIC EXCITATIONS

A. Experiments

Earlier studies of the magnetic excitations of HoP were performed on the single-crystal *S*1 which only exhibited short-range magnetic order presumably caused by Schottky defects.[12] Some years later inelastic neutron scattering experiments were carried out on the same polycrystalline sample *P*2 which was used for the neutron-diffraction study;[1] however, the instrumental energy resolution was not sufficient to reliably determine the magnetic excitation energies.[13] Now we have made a new attempt to measure the magnetic excitation spectrum of HoP by means of inelastic neutron scattering under improved experimental conditions for the polycrystalline sample *P*2 and the single-crystal *S*2 (see Table I and Sec. II A).

The inelastic neutron scattering experiments were performed at the DR3 reactor at Risø National Laboratory in Denmark using the triple-axis spectrometer TAS7 which is installed at a neutron guide connected to a cold H_2 source. The measurements were carried out in the neutron energy-loss configuration in the flopside phase ($1.5 \lesssim T \lesssim 2.2$ K). The analyzer energy was kept fixed at 4 and 5 meV for the measurements of the polycrystalline sample and the single crystal, respectively, and a beryllium filter cooled to liquid-nitrogen temperature was used to reduce higher-order contamination of the scattered neutron beam.

In Figs. 12 and 13 we show the resulting energy distributions of the scattered neutrons. Besides the elastic line which is almost entirely due to scattering from the vanadium container there is an intense double-peaked structure at 2 meV and a weaker line at 3 meV. A fourth inelastic peak appears as an unresolved shoulder on the low-energy side of the dominant inelastic line near 1.5 meV. The tails of the elastic peak extend up to an energy transfer of 1 meV; however, the symmetric shape of the elastic line (no excess intensity in the energy-loss part compared to the equivalent energy-gain part of the spectrum) suggests that there is no inelastic scattering in that region. In the data analysis the lines were approximataed by Gaussians. The results of the least-squares-fitting procedure are shown in Tables III and IV as well as by the solid lines in Figs. 12 and 13. The dashed lines indicate the background level and subdivision into individual lines.

B. Analysis of results

Following Kim and Levy[5] we describe the magnetic behavior of HoP by a Hamiltonian which contains crystal-field, bilinear, and quadrupolar pair interactions:

$$\mathcal{H}=\mathcal{H}_{\mathrm{CF}}-\sum_{i>j} J_{ij}\vec{\underline{S}}_i\cdot\vec{\underline{S}}_j - \sum_{i>j} K_{ij}\left[\tfrac{1}{3}\underline{Q}(\vec{S}_i)\underline{Q}(\vec{S}_j)+\underline{P}(\vec{S}_i)\underline{P}(\vec{S}_j)\right], \quad (1)$$

where

$$\underline{Q}(\vec{S}_i)=3\underline{S}_{iz}^2-S(S+1)$$

and

$$\underline{P}(\vec{S}_i)=\underline{S}_{ix}^2-\underline{S}_{iy}^2 .$$

Note that we have neglected the other three components

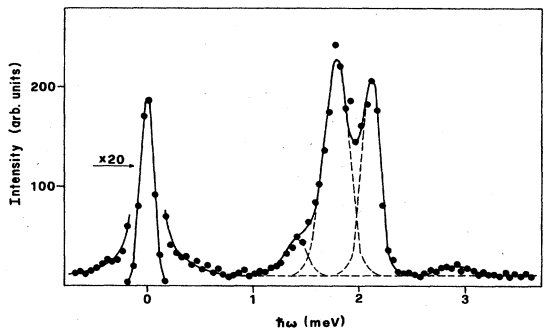

FIG. 12. Energy spectrum of neutrons scattered from polycrystalline HoP at $Q=1.34$ Å^{-1} and $T=2.2$ K. The lines are the results of a least-squares fit as explained in the text.

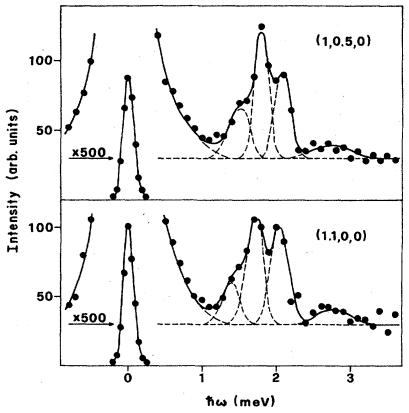

FIG. 13. Energy spectra of neutrons scattered from a single crystal of HoP at $T=1.5$ K for $\vec{Q}=(2\pi/a)\,(h,k,0)$. The lines are the results of a least-squares fit as explained in the text.

of the quadrupolar pair interactions, e.g., $\underline{S}_x\underline{S}_y-\underline{S}_y\underline{S}_x$, as we have anticipated using the cubic model in which these components are zero, see discussion below. In order to obtain a numerically tractable model we treat Eq. (1) in the mean-field approximation. This is a reasonable approximation, since there is no experimental evidence for dispersion effects in the magnetic excitation spectrum, see Fig. 13. Furthermore, we consider only the first- and second-neighbor bilinear interactions J_1,J_2 and first- and second-neighbor quadrupolar pair interactions K_1,K_2. We then obtain[5]

$$\mathcal{H}=\mathcal{H}_{\rm CF}-J\left\{(\vec{\xi}\pm\alpha\vec{\eta})\cdot\vec{\underline{S}}+\frac{a}{\sqrt{3}}(q_1\pm\alpha' q_2)\underline{Q}(\vec{S})+a(p_1\pm\alpha' p_2)\underline{P}(\vec{S})\right\}, \tag{2}$$

where the $\pm$ sign refers to the sublattice A or B, and the model parameters are defined by

$$\begin{aligned} J&=12J_1+6J_2\ ,\\ a&=(12K_1+6K_2)/J\ ,\\ \alpha&=-J_2/(2J_1+J_2) \end{aligned} \tag{3}$$

and

$$\alpha'=-K_2/(2K_1+K_2)\ .$$

Here J is the total bilinear coupling which sets the overall energy scale for the model, a is the total strength of the biquadratic interactions, and α,α' characterize the strengths of the antiferromagnetic and antiferroquadrupolar components of the interactions. The expectation values in Eq. (2) are defined by

$$\left.\begin{matrix}\vec{\xi}\\ \vec{\eta}\end{matrix}\right\}=\frac{\vec{M}_A\pm\vec{M}_B}{2}\ ,\qquad \left.\begin{matrix}q_1\\ q_2\end{matrix}\right\}=\frac{Q_A\pm Q_B}{2\sqrt{3}}\ ,\qquad \left.\begin{matrix}p_1\\ p_2\end{matrix}\right\}=\frac{P_A\pm P_B}{2}\ , \tag{4}$$

with

$$\vec{M}_A=\langle\vec{\underline{S}}_i\rangle\ ,$$

$$Q_A=\langle\underline{Q}(\vec{S}_i)\rangle\ ,$$

and

$$P_A=\langle\underline{P}(\vec{S}_i)\rangle\ ,$$

when i belongs to the sublattice A; similar definitions apply for the sublattice B. The flopside phase is characterized by

$$\vec{M}_A=(M_x,M_y,M_z)$$

and (5)

$$\vec{M}_B=(M_y,M_x,M_z)\ .$$

When Eq. (5) is valid, we have $Q_A=Q_B$ and $P_A=-P_B$, i.e., $q_2=p_1=0$, and we arrive at the following sublattice Hamiltonian for HoP in the flopside phase

$$\begin{aligned}\mathcal{H}_A=\mathcal{H}_{\rm CF}-6\{&[J_1M_x+(J_1+J_2)M_y]\underline{S}_x\\ &+[(J_1+J_2)M_x+J_1M_y]\underline{S}_y\\ &+(2J_1+J_2)M_z\underline{S}_z\}\\ &-2(2K_1+K_2)Q_A\underline{Q}(\vec{S})+6K_2P_A\underline{P}(\vec{S})\ .\end{aligned} \tag{6}$$

This Hamiltonian contains, besides $\mathcal{H}_{\rm CF}$, four parameters and five expectation values which have to be determined self-consistently. This is a difficult task if we have no prior knowledge about the model parameters. From neutron spectroscopy[3,4] we know that the crystal-field ground

TABLE III. Energies in meV and intensities of the magnetic excitations of polycrystalline HoP in the flopside phase at $T=2.2$ K.

	Energies		Intensities	
	Observed	Calculated	Observed	Calculated
E_5-E_1	1.42±0.10	1.34	0.12±0.04	0.10
E_6-E_1, E_3-E_1	1.79±0.02	1.62	1.00±0.15	1.00
E_4-E_1	2.11±0.03	2.06	0.59±0.10	0.45
E_2-E_1	2.92±0.10	2.91	0.05±0.03	0.02

TABLE IV. Observed energies in meV of the magnetic excitations of a single crystal of HoP in the flopside phase at $T=1.5$ K.

	$\vec{Q}=(2\pi/a)(1.1,0,0)$	$\vec{Q}=(2\pi/a)(1,0.5,0)$
E_5-E_1	1.40±0.10	1.50±0.10
E_6-E_1	1.72±0.03	1.80±0.02
E_3-E_1		
E_4-E_1	2.04±0.03	2.08±0.04
E_2-E_1	2.78±0.10	2.75±0.10

state is nearly sixfold degenerate, while the excited crystal-field states are at least 100 K above the ground state. Since the energies of the magnetic interactions are of the order of T_C, the dynamics of the spin system of HoP is essentially determined by the sixfold degenerate ground state. For this particular case one can make use of the "cubic model."[14] In this model the spin operators are projected onto the sixfold degenerate ground-state manifold; the crystal-field operator is a constant because the upper levels are neglected and the ground manifold is degenerate. For the sublattice A we have $M_x \gg M_y$ and $M_z=0$ for $T\rightarrow 0$, thus in a first approximation the eigenvalues of Eq. (6) are

$$\begin{aligned} E_1&=-6J_1-4K_1+4K_2\ , \\ E_2&=6J_1-4K_1+4K_2\ , \\ E_3&=-6J_1-6J_2-4K_1-8K_2\ , \\ E_4&=6J_1+6J_2-4K_1-8K_2\ , \\ E_{5,6}&=8K_1+4K_2\ , \end{aligned} \tag{7}$$

where we have used normalized spin operators $|\vec{\underline{S}}|=1$.

There is no straightforward way to attribute the observed lines to particular transitions between the states defined by Eqs. (7). This is made possible on the basis of the work performed by Kim and Levy who derived the following conditions for the model parameters:[5]

$$\begin{aligned} &J_1+J_2>0\ , \\ &2J_1+J_2>0\ , \\ &K_1+K_2<0\ , \\ &2K_1+K_2<0\ , \\ &J_1+J_2<-2(K_1+K_2)\ , \\ &2J_1-J_2>-2(2K_1-K_2)\ , \\ &2J_1+J_2>-4(2K_1+K_2)\ . \end{aligned} \tag{8}$$

From these conditions we conclude that the state with energy E_1 is the ground state, and we end up with three possible schemes. No one scheme is favored over the other two within the cubic-model approximation.

So far we have not made use of the intensities of the lines in the energy spectra. In order to do this one has to go beyond the cubic model because there are no dipole transition matrix elements between the six states in this model. Therefore we performed a full 17-level calculation on the basis of the Hamiltonian, Eq. (6).[15] In the calculation we took the three sets of parameters derived in the cubic-model approximation as starting values.

The crystal-field parameters[3,4] were kept fixed. It turned out that only one set of parameters was able to predict the correct intensities. These parameters were then varied until the best possible agreement was obtained between the spectroscopic data obtained from the polycrystalline sample and the calculated spectra; see Fig. 12. We found the following model parameters:

$$\begin{aligned} J_1&=0.24\pm0.01\ \text{meV}\ , \\ J_2&=-0.21\pm0.01\ \text{meV}\ , \\ K_1&=0.006\pm0.002\ \text{meV}\ , \\ K_2&=-0.043\pm0.002\ \text{meV}\ . \end{aligned} \tag{9a}$$

These yield

$$\begin{aligned} J&=1.62\pm0.18\ \text{meV}\ , \\ a&=-0.11\pm0.03\ \text{meV}\ , \\ \alpha&=0.78\pm0.12\ \text{meV}\ , \\ \alpha'&=-1.39\pm0.33\ \text{meV}\ . \end{aligned} \tag{9b}$$

The observed and calculated energies and intensities are summarized in Tables III and IV. While the lowest inelastic line corresponding to the splitting $E_{5,6}-E_1$ is doubly degenerate in the cubic model, the full 17-level scheme lifts this degeneracy and makes the level E_6 lie close to E_3. The corresponding splitting, however, could not be resolved in the experiments, and only an enhanced linewidth was observed. The peak identification is given in Tables III and IV.

Again it should be mentioned that the model parameters given above are "reduced parameters," i.e., they are obtained by using normalized spin operators $|\vec{\underline{S}}|=1$. This is also true for the interpretation of Eqs. (7) and (8). The actual model parameters J_i' and K_i' are obtained by using $|\vec{\underline{S}}|=8$ and given by

$$J_i'=J_i/8^2$$

and

$$K_i'=K_i/8^4\ . \tag{9c}$$

C. Discussion

No attempt was made in the present work to extend the inelastic neutron scattering experiments to higher-energy transfers, although a very intense line is expected to occur at around 10 meV. The position of this line, however, is a measure of the overall crystal-field strength; it does not contribute to a detailed understanding of the magnetic behavior of HoP at low temperatures.

Some measurements were also carried out in the ferromagnetic phase. The observed energy spectra, however, have the shape of a broad quasielastic line and consequently are not suited for a detailed analysis. This is a consequence of the fact that in the ferromagnetic phase

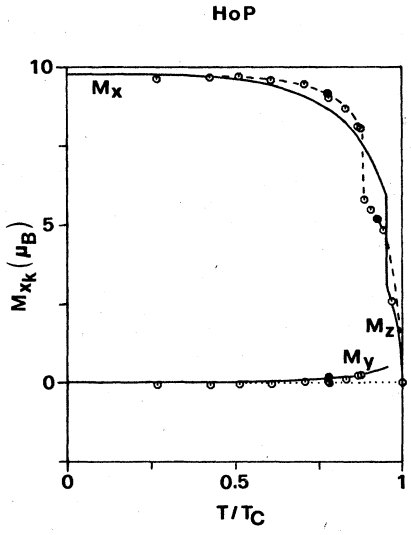

FIG. 14. Dependence of the order parameter $\vec{M}$ of the Ho^{3+} ions in HoP on temperature. The circles represent the experimental data, see Fig. 3. The solid line corresponds to the values calculated from the model parameters. The dashed line is a guide to the eye.

the spin waves are overdamped, because the system is far from saturation.

We used the model parameters determined from the magnetic excitation spectra to calculate the temperature dependence of the order parameters of Ho^{3+} in HoP. The results for $\vec{M}$ obtained by using the full crystal-field level scheme are shown in Fig. 14. Results based on the cubic model, i.e., six degenerate ground states, give nearly identical results. The calculations were performed both for the flopside and the ferromagnetic phase in order to decide which solution is energetically more favorable. For the ferromagnetic phase we have $\vec{M}=(0,0,M_z)$, $Q_A=Q_B$,

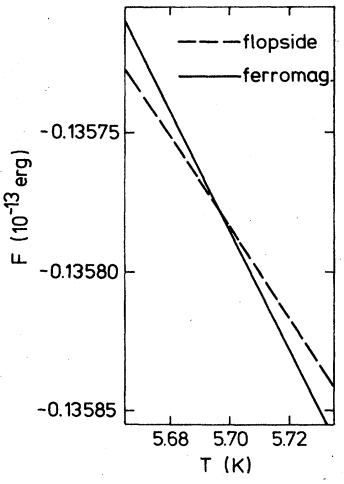

FIG. 15. Temperature dependence of the free energies of the flopside and ferromagnetic phases in zero field. As the slope of the flopside phase is less than that for the ferromagnetic phase at T_F, we find the entropy of the flopside phase is less than that of the ferromagnetic phase at T_F. Note: $S=-\partial F/\partial T$.

and $P_A=P_B=0$; thus the Hamiltonian Eq. (2) reads

$$\mathcal{H}=\mathcal{H}_{\mathrm{CF}}-6(2J_1+J_2)M_z\underline{S}_z-2(2K_1+K_2)Q_A\underline{Q}(\vec{S})\ . \tag{10}$$

The temperature dependence of the free energy predicts a transition from the flopside to the ferromagnetic phase at $T_F=5.7$ K, see Fig. 15. The discontinuities in the order parameters found in our calculation indicate that this transition is first order, whereas the transition from the ferromagnetic to the paramagnetic phase at $T_C=6.0$ K is second order. Thus the model can qualitatively account for all the features of the zero-field magnetization determined by neutron diffraction. The difference between theory and experiment is that the model predicts transition temperatures which exceed the observed transition temperatures by about 20%. However, a discrepancy of this order of magnitude should be expected from the mean-field approximation.

IV. PHASE DIAGRAMS FOR FINITE FIELDS

We have just seen that the model Hamiltonian Eq. (1) together with the parameters determined from the magnetic excitation spectrum is able to account for the spontaneous magnetization (zero field) of HoP as a function of temperature. To further test the ability of this Hamiltonian and the parameters to reproduce the magnetothermal behavior of HoP we will compare the field-temperature phase diagrams found by using them and mean-field theory to the experimental data in Sec. II. We will limit our discussion to a model with only tow sublattices. Each sublattice represents ferromagnetic (111) planes of spins pointing along one of the cube axes: x, y, or z. It is conceivable that in certain directions of the field a multisublattice structure is more stable but we have not considered this in the present analysis.

For small fields[16] the nature of these diagrams depends critically on the orientation of the external field relative to the crystal axes, because of the relatively strong crystal-field anisotropy. This anisotropy is such as to rigidly orient the magnetic moments along one of the cube edges $\langle 100\rangle$. When the external field makes an angle with respect to the cube edges the magnetization does not follow. In the magnetically ordered phase the best HoP can do is to break up into sublattices with each moment pointing along a different cube edge, i.e., in such a configuration that the resultant magnetization has its maximum projection along the field.

In the presence of a field, the paramagnetic phase is characterized by the magnetization having components of the form (M,M,M) for $\vec{H}\|[111]$, $(M,M,0)$ when $\vec{H}\|[110]$, and $(M,0,0)$ for $\vec{H}\|[100]$. However, when $\vec{H}\|[11a]$ $(0<a<1)$, the paramagnetic state has $\vec{M}=(M,M,M')$ where M' is not necessarily $M'=aM$, i.e., $\vec{M}$ *may not be parallel to* $\vec{H}$. For example, when $H\rightarrow\infty$ (remaining within our rigid cubic model) $\vec{M}=(\frac{1}{2},\frac{1}{2},0)$ regardless of $(a<1)$ since any spin going out of x or y direction must overcome infinite magnetic energy.

When there is a small magnetic field $\vec{H}$ in our model of HoP (Ref. 5) the direction of the magnetization in the fer-

romagnetic phase will be along one of the six cube edges depending on the relative magnitudes of H_x, H_y, and H_z. For example, when $H_x > |H_y|$ or $H_x > |H_z|$, it will be [100]. Therefore, in the $(T,\vec{H})$ phase space the $H=0$ line for $T_F < T < T_C$ will be the coexistence line for *six* phases. Likewise, for $T < T_F$ 12 phases whose net magnetizations are along [110], $[1\bar{1}0], \ldots, [0\bar{1}\bar{1}]$, respectively, coexist on the $H=0$ line. Therefore, for $H=0$, when we say that the [001] ferromagnetic phase goes into the xy flopside phase[12] we really mean that it goes into any one of the 12 possible flopside phases. However, if there is a small field, say H_z, the ferromagnetic phase along [001] would go into one of the four flopside phases (xz), $(\bar{x}z)$, (yz), or $(\bar{y}z)$.

The qualitative features of the temperature-field phase diagrams can be obtained analytically for the regions along the temperature axis for small fields and along the field axis at zero temperature. Near the flopside transition ($T \simeq T_F$) and to first order in the field we can write the free energy as

$$F(T,\vec{H}) = F(T,0) - \vec{M}(T)\cdot\vec{H} + O(H^2) , \tag{11}$$

where $\vec{M}(T)$ is the uniform magnetization per spin in zero field. When $T = T_F + \epsilon$ ($\epsilon \ll 1$), we find

$$F(T_F+\epsilon,\vec{H}) = F(T_F,0) - S(T_F)\epsilon - \vec{M}(T_F)\cdot\vec{H} , \tag{12}$$

where $S(T_F) = (-\partial/\partial T)F(T_F,0)$ is the entropy in zero field and at $T=T_F$. For $H=0$ and $T=T_F$ many phases coexist, i.e., many phases with the same free energy $F(T_F,0)$ but different S and $\vec{M}$. As we apply a field, coexistence surfaces grow and their location $\epsilon(\vec{H})$ is determined by the condition that the free energies, Eq. (12), are the same. Thus, the condition for a phase transition is

$$\begin{aligned} F_1(T_F+\epsilon,\vec{H}) - F_2(T_F+\epsilon,\vec{H}) \\ = 0 = F_1(T_F,0) - F_2(T_F,0) - [S_1(T_F) - S_2(T_F)]\epsilon \\ - [\vec{M}_1(T_F) - \vec{M}_2(T_F)]\cdot\vec{H} , \end{aligned} \tag{13}$$

where 1 refers to the ferromagnetic or paramagnetic phase and 2 refers to the flopside phase. As the free energies of the ferromagnetic and flopside phases in zero field are equal at T_F by definition, we find

$$\left.\frac{dH}{dT}\right|_{\text{cxs}} = \frac{S_1 - S_2}{(\vec{M}_2 - \vec{M}_1)\cdot\hat{H}} , \tag{14}$$

where we set $\epsilon = dT$, $\vec{H} = dH\,\hat{H}$, and the subscript cxs means along the coexistence line.

Near T_F and for $H=0$ the magnetization and free energy of the ferromagnetic and flopside phases have the behaviors shown in Figs. 14 and 15. As the slope of the free energy versus temperature is smaller for the flopside phase we can see that at T_F the entropy of the flopside phase is less than that of the ferromagnetic phase. Numerical calculations based on our model using the full 17-level scheme yield at T_F and $H=0$: $S(\text{ferro}) = 1.56k_B$, $S(\text{flop}) = 1.18k_B$, $M_z(\text{ferro}) = 3.0\mu_B$, $M_x(\text{flop}) = 5.8\mu_B$, and $M_y(\text{flop}) = 0.5\mu_B$. As can be seen from these numbers, for certain orientations of the field the denominator in Eq. (14) will be the small difference between large numbers. Thus the slope dH/dT depends crucially on this difference. Also, the entropy has been estimated by taking the difference of the free energy at low temperature. Since the mean-field approximation is not particularly reliable for quantitative results, the numerical value of the slopes obtained by using the above numbers cannot be expected to be accurate. Nonetheless, as we now show we obtain qualitative predictions, from Eq. (14), of how the slope dH/dT varies with the direction of the field, which are borne out by the experiments described in Sec. II.

For fields along the cube edge $\hat{H} = [001]$, the "ferromagnetic" phase[17] (001) and the flopside phases $(yz),(\bar{y}z),(xz),(\bar{x}z)$ come into play. The component of the magnetization along the field in the flopside phase is

$$M_z^{(\text{flop})} = \tfrac{1}{2}(M_x + M_y) , \tag{15}$$

and the denominator in Eq. (14) is $0.15\mu_B$. This is indeed a small difference of much larger numbers, and yields a slope, for the field along $\langle 001 \rangle$, of

$$\left.\frac{dH}{dT}\right|_{\text{cxs}}^{\langle 001\rangle} = 43 \text{ kOe/K} , \tag{16}$$

in approximate agreement with the experimental value; see Fig. 6.

For a field

$$\vec{H} = \frac{H}{(2+a^2)^{1/2}}(1,1,a) ,$$

as long as $|a| < 1$, the ferromagnetic phase with order parameter $(M_z 00)$ (in zero field) coexists with the flopside phase $[(M_x+M_y)/2,(M_x+M_y)/2,0]$ at $T=T_F$.[18] By using the numerical values found from our model we find that the initial slope of the flopside ferromagnetic coexistence line is

$$\begin{aligned} \left.\frac{dH}{dT}\right|_{\text{cxs}}^{\langle 110\rangle} &= 2.0(2+a^2)^{1/2} \text{ kOe/K} \\ &= \begin{cases} 2.8 \text{ kOe/K for } a=0 , \\ 3.5 \text{ kOe/K for } a \simeq 1 . \end{cases} \end{aligned} \tag{17}$$

This slope is typically one-tenth as large compared to the slope in the [001] direction. By comparing the slopes in the phase diagrams for $\vec{H}||[001]$ and $[0\bar{1}1]$, see Figs. 6 and 7, we confirm that the slope is much steeper for fields along [001].[19]

At *zero* temperature we can determine the field at which the flopside phase stable in zero field goes over to the "ferromagnetic"[17] phase. By including a Zeeman energy term in our simplified six-level model of HoP,[5] the ground-state energy is

$$U = -\tfrac{1}{2}J(\xi^2 + \alpha\eta^2 + a\gamma^2 + a\alpha'\delta^2 + \vec{h}_0\cdot\vec{\xi}) , \tag{18}$$

where

$$\left.\begin{matrix}\gamma^2 \\ \delta^2\end{matrix}\right\} = \left[\frac{1}{2\sqrt{3}}(Q_A \pm Q_B)\right]^2 + \tfrac{1}{4}(P_A \pm P_B)^2 ,$$

$$h_0 \equiv 10\mu_B H_0 / \tfrac{1}{2}J ,$$

and the M_α, Q_α, P_α, ξ, and η are defined by Eq. (4). In our definition of h_0 we used $g_J=\frac{5}{4}$ for the $J=8$ state of Ho^{3+}.

For a field along [001] the energy of the flopside phase (xz) is

$$U_{xz}=-\tfrac{1}{2}J[\tfrac{1}{2}(1+\alpha)+a(\tfrac{1}{3}+\alpha')+\tfrac{1}{2}h_0]\ , \tag{19}$$

while for a "ferromagnetic" phase [001] the energy in a field is

$$U_{zz}=-\tfrac{1}{2}(1+\tfrac{4}{3}a+h_0)\ . \tag{20}$$

When the energies of the two phases are equal they coexist and we find the critical field at $T=0$ K to go from the flopside to ferromagnetic phase by equating Eqs. (19) and (20),

$$h_c=(\alpha-1)+2a(\alpha'-1)\ . \tag{21}$$

By using the parameters found from the magnetic excitation spectrum, see Sec. III, we find

$$H_c=4.28\text{ kOe}\ . \tag{22}$$

However, numerical calculations of the free energies of the flopside and ferromagnetic phases at $T=2$ K based on the full 17-level scheme yield $H_c\cong 12.3$ kOe. This is in much better agreement with the experimental results shown in Fig. 6.

For directions of $\vec{H}$ other than $\langle 100\rangle$ the situation is more complicated. Let us consider $\vec{H}||[11a]$ $(0\le a<1)$ and $T_F<T<T_C$. In this case the magnetization is $(M,0,0)$ for $H=0$. When a small field is present, $\vec{M}$ grows starting from its zero-field value but with different rates for each direction. Therefore, a phase with $\vec{M}=(M_x,M_y,M_z)$ where $M_x>M_y\simeq M_z$ can exist. Since there is a symmetry between the y and z axes for $H=0$ ($\vec{M}$ is along the x direction), we expect that the zero-field susceptibility is the same for the y and z directions; and $M_z\simeq aM_y$ for small fields. This phase is what we call the ferromagnetic phase: As temperature is lowered the symmetry $M_x=M_y$ present in the paramagnetic phase is broken at $T_C(H)$ and the system goes into a state where $M_x>M_y$. Therefore the transition at $T_C(H)$ should be of the Ising universality class, i.e., a second-order transition with Ising-like critical behavior.

Specifically for $a=0$, i.e., for $\vec{H}||[110]$, the ferromagnetic phase has a magnetization of the form $(M_x,M_y,0)$ with $M_x>M_y$. When $\vec{H}||[111]$, the ferromagnetic state has a magnetization of the form (M_x,M_y,M_z) with $M_x>M_y=M_z$. The transition from the paramagnetic to the ferromagnetic phase breaks the symmetry between the x, y, and z directions and one of the directions, say x, is preferred. Therefore the transition in a field $\vec{H}||$ [111] is of the three-state Potts-model universality class and we expect a first-order transition for $d=3$.

These ferromagnetic phases disappear in relatively weak fields at least in the mean-field approximation (MFA). For $\vec{H}||\langle 110\rangle$ or $\vec{H}||\langle 11\frac{1}{3}\rangle$, $\bar{H}=0.02$ ($H=0.56$ kOe), while for $\vec{H}||\langle 111\rangle$, $H=0.01$ ($H=0.28$ kOe). Note $\bar{H}=10\mu_B H/J$.

To obtain more details of the phase diagrams away from the temperature ($H=0$) and field ($T=0$) axes it was necessary to numerically solve the mean-field equations for the free energy of our system in a field. In our calculations we used the cubic model[5] with the parameters found in Sec. III. The results of our analyses are summarized in Fig. 16, where we show the regions where the paramagnetic, ferromagnetic, and flopside phases exist and the lines of coexistence between them.

For $\vec{H}||\langle 100\rangle$ we find the diagram shown in Fig. 16(a). This is as expected and qualitatively similar to the experimental data, although our curve is more rounded near T_F. The transition is first order everywhere. It intercepts the $T=0$ axis at $\bar{H}=0.153$ ($H=4.28$ kOe). The initial slope at $H=0$ is positive but soon curves around.

For $\vec{H}||\langle 110\rangle$ or $\langle 11\frac{1}{3}\rangle$, see Figs. 16(b) and 16(c), the ferromagnetic-to-paramagnetic transition is second order. When H tends to zero $T_C(H)$ behaves like

$$\bar{T}_C(H)=\bar{T}_C(0)-\text{const}\times H^{3/2}$$

$$=\tfrac{1}{3}-\alpha H^{3/2}\ . \tag{23}$$

The ferromagnetic-to-flopside transitions and the paramagnetic-to-flopside transitions for low fields are first order. The paramagnetic-to-flopside transitions for $\bar{H}>0.07$ for $\vec{H}||\langle 110\rangle$ and $\bar{H}>0.09$ for $\vec{H}||\langle 11\frac{1}{3}\rangle$ are second order. However, the appearance of a line of second-order transitions in high fields seems to be an artifact of using the mean-field approximation: When H tends to infinity and $\vec{H}||\langle 11a\rangle$ the cubic model reduces to an Ising model, and the corresponding Ising Hamiltonian is

$$H_{\text{eff}}=-\bar{J}_1\sum_{\text{NN}}\sigma\sigma'+\lambda\bar{J}_1\sum_{\text{NNN}}\sigma\sigma'\ , \tag{24}$$

where $\bar{J}_1=0.126$ meV, $\lambda=1.16$, NN denotes nearest neighbor, and NNN denotes next-nearest neighbor. Here $\sigma_i=+1$ (-1) corresponds to $\vec{S}_i=[100]$ ([010]). The flopside phase corresponds to a type-II antiferromagnetic phase of this Ising model, and simple mean-field theory predicts a second-order phase transition at $k_BT_C=6\lambda\bar{J}_1$, or $k_BT_C/J=0.543$ ($J=1.62$ meV). However, this model is sufficiently simple and we have extended our investigation in two ways.[20]

First we made a Monte Carlo simulation for a $20\times20\times20$ system of spins. This predicts a *first-order* transition at $k_BT_C/J=0.3\pm0.05$. Second we used a correlated mean-field theory.[20] This also predicts a first-order transition at $k_BT_C/J=0.311$ ($J=1.62$ meV) or $T_C\simeq5.8$ K.

These two results strongly suggest that in better approximations our cubic model should have a line of first-order transitions all the way up to $H=\infty$. Furthermore the correction to T_C of the Ising model from the MFA is *drastic*. Therefore, when better approximations are used to solve our cubic model we expect the phase diagrams in Fig. 16 will look more like those found experimentally, see Figs. 6 and 7.

Finally for the field along $\vec{H}||\langle 111\rangle$, see Fig. 16(d), all transitions are first order. The limit $H\to\infty$ in this case reduces our system to the three-state Potts model and a first-order transition is expected. Also, the ferromagnetic-to-paramagnetic transition is first order as

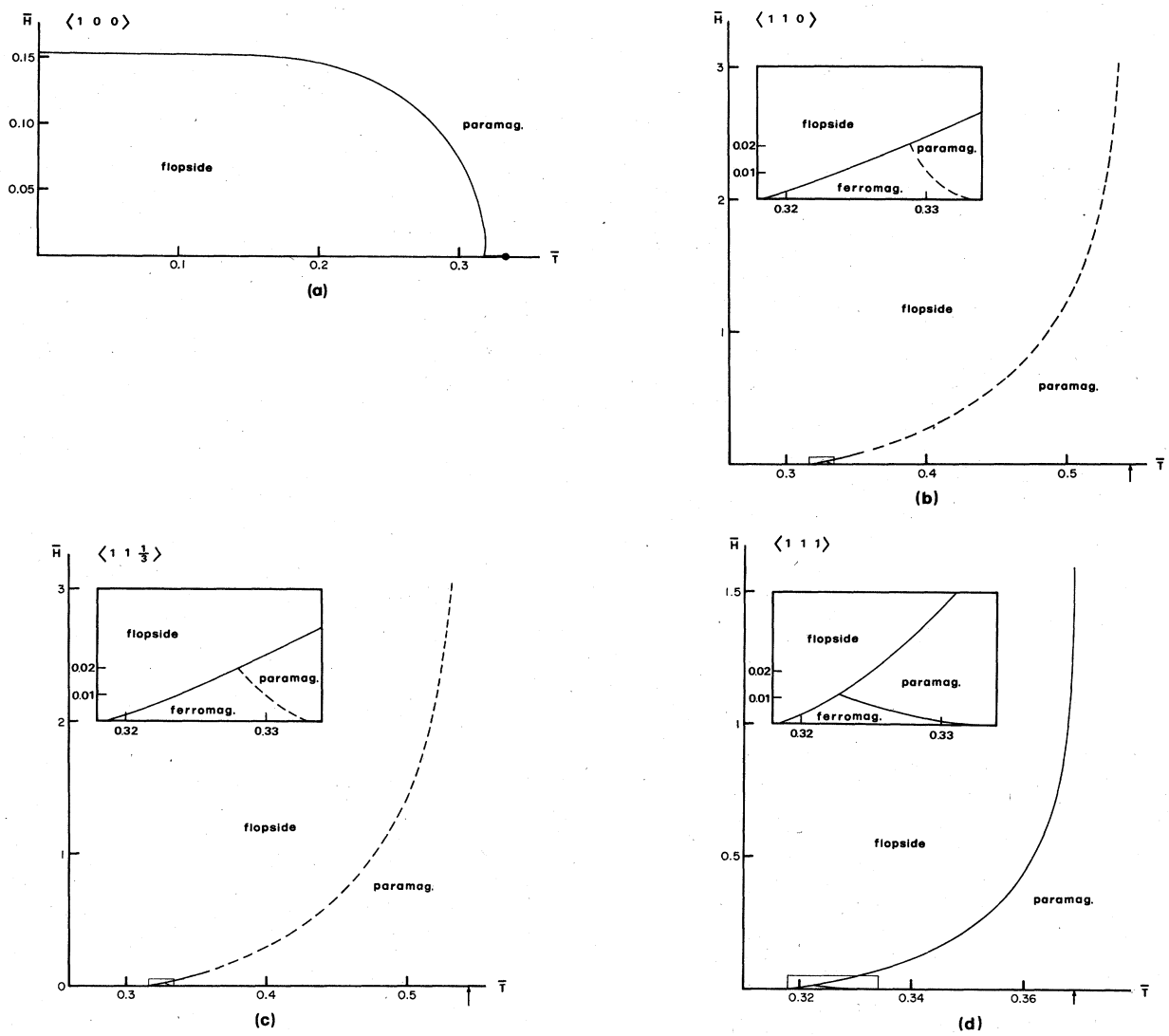

FIG. 16. Phase diagrams for different directions of the magnetic field found by using the cubic model; see Ref. 5 with the parameters found in Sec. III, $J=1.62$ meV, $\alpha=0.78$, $a=-0.11$, and $\alpha'=-1.39$. Solid lines denote first-order transitions; dashed lines denote second-order transitions. The fields and temperatures are given in terms of the reduced units $\overline{H}\equiv 10\mu_B H/J$ and $\overline{T}=kT/J$. $\overline{T}_F(H=0)=0.318$ and $\overline{T}_C(H=0)=0.333$. The insets are enlargements of the areas indicated by the boxes near the $H=0$ axes. The arrows on the $\overline{T}$ axes indicate the value of T_F when $H=\infty$. This value is significantly lower in better approximations as discussed in Ref. 20.

can be seen from symmetry arguments.

From the variation of the magnetization versus temperature it is not possible to tell whether the transitions in finite fields are first or second order. In zero field, see Figs. 3 and 4, it is obvious that the flopside transition is first order as the magnetization is discontinuous. However in finite fields the fact that the samples contain differently oriented domains means that the field is oriented in different directions for the various domains. This causes the transition to be smeared out, and it is not possible at present to unequivocally identify the order of the phase transitions in a field; see Fig. 8.

V. SUMMARY

We have shown, that the model Hamiltonian proposed for HoP in zero field also is able to reproduce the qualitative feature of its phase behavior in fields. Because of the strong anisotropy present in this system the phase behavior depends on the direction of the field with respect to the crystal axes. For fields along ⟨100⟩ the flopside phase goes over to a ferromagnetic phase at sufficiently high fields, while for fields along ⟨11a⟩ the flopside phase is stable for all fields at low temperature. Also, we find the slope of the coexistence line $dH/dT\,|_{\rm cxs}$ is much steeper in the ⟨100⟩ directions than in the ⟨11a⟩ directions. These features of the phase diagrams have been confirmed by the new neutron scattering studies reported here. Quantitative estimates of the transition temperature as a function of field were made by using the parameters determined from an analysis of the magnetic excitation spectrum of HoP. These parameters correctly predict that in zero field HoP has first a second-order paramagnetic-

to-ferromagnetic transition followed by a first-order ferromagnetic-to-flopside transition. The transition temperatures are reasonably well described by these parameters (to within 20%).

While the cubic model is quite good in predicting the properties of HoP in *zero* field, it is of limited value in predicting the phase behavior of HoP in a field. As we have seen in Sec. IV the phase diagrams found from the cubic model, Figs. 16, have features that are qualitatively similar to the experimental diagrams; see Figs. 6 and 7. However, the estimate of the flopside-to-ferromagnetic transition temperature, Eq. (22), and other quantitative features of the phase diagrams based on calculations using the cubic model are off by factors of 2 to 3. When we used the full 17-level scheme to calculate this transition temperature the agreement was much better. In addition, the slopes $dH/dT\,|_{\text{cxs}}$ obtained by using Eq. (14) are quite close to those observed when we use the entropies and magnetic moments determined from the *full* 17-level calculation.

Finally, for fields along $[0\bar{1}1]$ it has been found that the $[1\bar{1}1]$ domain is preferred, i.e., more stable than the [111] domain and they produce different phase boundaries. This can be seen from Fig. 7 where we see that the reflection $\frac{1}{2}\frac{1}{2}\frac{1}{2}$ from the [111] domain disappears in fields above 10 kOe. Our model Hamiltonians, Eqs. (2) or (6), do not favor one domain over the other. This is probably due to our neglecting the two-ion magnetoelastic interactions between the holmium ions.[21] In the magnetically ordered phase these interactions produce anisotropic pair interactions which may yield different energies for the [111] and $[1\bar{1}1]$ domains in field along $[0\bar{1}1]$.

ACKNOWLEDGMENTS

We would like to thank A. Wisard for his help in preparing the samples. This work was supported in part by the Research Institute for Basic Sciences of Seoul National University (D.K.), and by a grant from the National Science Foundation, No. DMR-81-20673 (P.M.L.).

[1]P. Fischer, W. Hälg, and E. Kaldis, J. Magn. Magn. Mater. **14**, 301 (1979); P. Fischer, W. Hälg, E. Kaldis, F. J. A. M. Greidanus, and K. H. J. Buschow, in *Neutron Scattering—1981 (Argonne National Laboratory)*, proceedings of the Symposium on Neutron Scattering, Argonne, 1981, edited by J. Faber, Jr. (AIP, New York, 1982), p. 321.

[2]H. R. Child, M. K. Wilkinson, J. W. Cable, W. C. Koehler, and E. O. Wollan, Phys. Rev. **131**, 922 (1963).

[3]R. J. Birgeneau, E. Bucher, J. P. Maita, L. Passell, and K. C. Turberfield, Phys. Rev. B **8**, 5345 (1973).

[4]A. Furrer and E. Kaldis, in *Magnetism and Magnetic Materials—1975 (Philadelphia)*, proceedings of the 21st Annual Conference on Magnetism and Magnetic Materials, edited by J. J. Becker, G. H. Lander, and J. J. Rhyne (AIP, New York, 1976), p. 264; K. R. Lea, M. J. M. Leask, and W. P. Wolf, J. Phys. Chem. Solids **23**, 1381 (1962).

[5]D. Kim and P. M. Levy, J. Magn. Magn. Mater. **27**, 257 (1982).

[6]E. Kaldis, *Crystal Growth Theory and Techniques 1*, edited by C. H. I. Goodman (Plenum, New York, 1974), p. 47; E. Kaldis, J. Cryst. Growth **24/25**, 53 (1974).

[7]H. M. Rietveld, J. Appl. Cryst. **2**, 65 (1969).

[8]L. Koester and W. B. Yelon, Neutron Diffraction Newsletter, 1983 (unpublished).

[9]A. J. Freeman and J. P. Desclaux, J. Magn. Magn. Mat. **12**, 11 (1979).

[10]P. Fischer, P. Schobinger-Papamantellos, and E. Kaldis, in *Proceedings of the Discussion Meeting on Magnetic Semiconductors, Jülich*, edited by W. Zinn (North-Holland, Amsterdam, 1976), p. 200.

[11]G. Busch, P. Schwob, and O. Vogt, Phys. Lett. **23**, 636 (1966).

[12]A. Furrer, P. M. Levy, and E. Kaldis, *Crystal Field Effects in Metals and Alloys*, edited by A. Furrer (Plenum, New York, 1977), p. 24.

[13]A. Furrer and E. Kaldis, *Crystalline Electric Field and Structural Effects in f-Electron Systems*, edited by J. E. Grow, R. P. Guertin, and T. W. Mihalisin (Plenum, New York, 1980), p. 497.

[14]D. Kim, P. M. Levy, and L. F. Uffer, Phys. Rev. B **12**, 989 (1975).

[15]H. H. Chen and P. M. Levy, Phys. Rev. B **7**, 4267 (1973).

[16]When the fields are extremely large, i.e., when they overcome the crystal-field anisotropy, which is of the order of several hundred degrees Kelvin, HoP behaves like a paramagnet. However, we limit our discussion to fields small compared to the crystal field, so that we can limit ourselves to the sixfold nearly degenerate, ground manifold.

[17]The ferromagnetic phase exists only in zero field for $\vec{H}||\langle 100\rangle$. For $\vec{H}||[100]$ the magnetization is of the form $(M',0,0)$ and there is no clear distinction between the paramagnetic and ferromagnetic phases. The phase diagram has a coexistence line sticking out from T_F to T_C along $H=0$.

[18]In the flopside phase one sublattice is $\vec{M}_A=(M_x,M_y,0)$ while the other is $\vec{M}_B=(M_y,M_x,0)$. A uniform field sees the average $\frac{1}{2}(\vec{M}_A+\vec{M}_B)$ per spin.

[19]If one used the values of the magnetization at T_F and $H=0$ found from neutron scattering experiments, i.e., $M_x=8.1\mu_B$, $M_y=0.2\mu_B$, and $M_z=5.8\mu_B$, we would find $(dH/dT)_{\langle 001\rangle}<0$. This negative slope in the $\langle 001\rangle$ directions is in contradiction with the observed phase diagram, see Fig. 6. Either $[\frac{1}{2}(M_x+M_y)-M_z]$ should be positive or the experimental phase diagram [001] should have a negative initial slope.

[20]J. Y. Lee and D. Kim (unpublished); T. Kaneyoshi, J. Magn. Magn. Mater. **15-18**, 119 (1980); D. C. Mattis, Phys. Rev. B **19**, 4737 (1979); H. I. Zhang and D. Kim, *ibid.* **21**, 4173 (1980).

[21]G. Lacueva, P. M. Levy, and P. Morin (unpublished).